Wood Sci Technol (2010) 44:67–84
DOI 10.1007/s00226-009-0257-2

ORIGINAL

Application areas of synchrotron radiation tomographic microscopy for wood research

David Mannes · Federica Marone · Eberhard Lehmann · Marco Stampanoni · Peter Niemz

Received: 18 August 2008 / Published online: 3 June 2009

Abstract Possible applications for synchrotron radiation tomographic microscopy in the field of wood research were tested and evaluated at the TOMCAT beamline (TOmographic Microscopy and Coherent rAdiology experimenTs) at the Swiss Light Source (SLS) at the Paul Scherrer Institute (Villigen, Switzerland). For this study, small cylindrical samples (∅ 1 and 3 mm) were examined with different experimental setups resulting in a nominal voxel size of approximately 1.48 × 1.48 × 1.48 and 3.7 × 3.7 × 3.7 μm^3, respectively. Suitability of the TOMCAT microscope for 3D investigations of wood anatomy was tested on several softwood and hardwood species revealing microscopic features (e.g. tyloses, wall thickenings or pits) down to the nominal pixel size. The results suggest that even features in the sub-voxel range can be made visible. Tomographic microscopy was also tested for wood technological applications, i.e. penetration behaviour of a wood preservative and also of three wood adhesives (poly-urethane resins) with different viscosities. Although the experiments with the preservative yielded no clear results, the method seems suitable for examining the penetration of the different adhesives. The adhesive penetrates the wood mainly by the vessels where it can be easily discerned from the wood structure.

D. Mannes · P. Niemz
Department of Civil, Environmental and Geomatic Engineering, Institute for Building Materials, ETH Zurich, 8093 Zurich, Switzerland

F. Marone · M. Stampanoni
Swiss Light Source (SLS), Paul Scherrer Institut (PSI), 5232 Villigen, Switzerland

D. Mannes (✉) · E. Lehmann
Spallation Neutron Source (ASQ), Paul Scherrer Institut (PSI), 5232 Villigen, Switzerland
e-mail: dmannes@ethz.ch

M. Stampanoni
Institute for Biomedical Engineering, University and ETH Zurich, 8092 Zurich, Switzerland

Introduction

Wood is a natural, organic material with a complex structure, which is very distinctive over several hierarchical levels: from the macroscopic (e.g. annual ring structure) over the mesoscopic (alignment of different tissues) and microscopic (e.g. cell features) down to the submicroscopic level (e.g. cellulose-fibrils). Wood properties depend on the anatomical features of the different hierarchical levels. This study focuses on the microscopic level, evaluating synchrotron radiation micro computer tomography (SRμCT) as an alternative non-destructive method to standard microscopy in the field of wood research. For investigations on this level, classic methods like light or electron microscopy imply the partial destruction of the sample, always bearing the risk of preparation artefacts. Moreover, these methods only yield 2D information of a certain area. There have been attempts to extend these methods to 3D by using confocal laser scanning microscopes (CLSM, Knebel and Schnepf 1991) or by producing serial sections of a sample and scrutinising them with a light microscope (Dodd 1948). But these approaches necessitate either a very complicated, time-consuming and error-prone sample preparation in the case of serial sections or only allow a restricted inside view with a depth of generally <200 μm in the case of CLSM (Donaldson and Lausberg 1998; Kitin et al. 2003, 2004).

One way to avoid these issues can be the utilisation of non-destructive testing methods. Bucur (2003a, b) gives a general overview on this subject. For investigations on the microscopic level, computed tomography using ionising radiation seems the most promising way. While γ-rays (with a spatial resolution in the millimetre-range) can be used to characterise the wood density only on the macroscopic level (e.g. Macedo et al. 2002) and as the handling of radioactive sources can be problematic, neutron and X-ray radiation seem more appropriate. Neutron tomography shows a very high contrast for hydrogen. It is thus particularly suited for investigations on the interaction of wood with other hydrogen-containing materials like adhesives, preservatives, coatings or water (Niemz et al. 2004). Due to the resolution of 30–50 μm, this method is on the edge between the mesoscopic and microscopic level (Mannes et al. 2007).

With X-rays, the microscopic level can be reached as shown by Steppe et al. (2004) who studied anatomical wood features non-invasively using a micro-focus X-ray tube. Van den Bulcke et al. (2008) used a similar setup with a nano-focus X-ray tube, which allowed them to analyse infested wood down to a voxel size of around 1 μm.

A better contrast and even higher resolution can be achieved using synchrotron light. A synchrotron source, like the Swiss Light Source (SLS) at the Paul Scherrer Institute (PSI) in Villigen (Switzerland), yields electromagnetic radiation, e.g. X-rays, characterised by a much higher brilliance, which allows investigations in ever smaller orders of magnitude.

Trtik et al. (2007) showed the applicability of SRμCT in "phase-contrast mode" for the 3D imaging of spruce wood, achieving a nominal voxel size of $0.7 \times 0.7 \times 0.7\ \mu m^3$ allowing the resolution of structures down to approximately

1.5 μm. The "phase-contrast mode" (Groso et al. 2006) uses the phase shift of the beam caused by refraction in the sample, which enhances the contrast and can be advantageous if materials with low absorption contrast are examined. Since the mentioned investigations of Trtik et al. (2007), a new beamline dedicated to tomographic microscopy, named TOMCAT (**TO**mographic **M**icroscopy and **C**oherent r**A**diology experimen**T**s) (Stampanoni et al. 2007), has been built at the SLS, which allows 3D-imaging experiments either in traditional absorption based or phase-contrast mode.

The presented work was conceived to continue the SRμCT experiments on wood using the new TOMCAT beamline. The aim of this study was to evaluate the suitability of the method for different topics within the field of wood research using absorption-based tomography. For this purpose, a variety of different samples was selected to cover a wide range of possible applications, including investigations on microscopic wood features as well as wood technological questions like the penetration behaviour of adhesives.

Experimental

Materials

In order to minimise the risk of artefacts during the reconstruction of the tomography data, a cylindrical specimen shape was chosen (∅ 1 or 3 mm; length 10–15 mm). The samples were produced using a metal turning lathe.

Before and after the machining as well as before the experiment itself, the samples were stored in ambient room climate (ca. 20°C/40–50%RH), which was the same as during data acquisition. In this way, possible changes of the moisture content resulting in swelling or shrinkage during the measurement were avoided, ensuring high-quality results.

For the first part of the experiment, where the suitability of the TOMCAT microscope for studying anatomical wood features was to be evaluated, untreated specimens of three softwoods and two hardwoods were selected (cf. Table 1). The chosen wood samples guaranteed a relatively broad variety of species (with beech and spruce being the most common ones in Europe).

In the second part of the investigations, more technological issues were studied. In a first step, the penetration behaviour of a wood preservative (containing Ag-nano-particles, *Nano-Perl*® as main agent) in and perpendicular to the fibre direction was scrutinised. For this purpose, spruce and beech cubes ($5 \times 5 \times 5$ cm^3) were pressure impregnated with the agent and the cylindrical samples were produced from the said cubes (cf. Table 1).

The last part of the investigation had its focus on the penetration behaviour of wood adhesives. Beech wood samples had been glued beforehand with different poly-urethane resins (PUR) showing varying viscosities. In the finished samples the glue line was oriented central along the axes dividing the specimen in two half cylinders.

Table 1 Overview of the samples used in the experiments

Category	Wood species	∅ (mm)	Remarks
Microscopic wood anatomy	European Beech (*Fagus sylvatica*)	1	
		3	
	Oak (*Quercus* sp.)	3	
	Norway spruce (*Picea abies*)	1	
		3	
	Scots pine (*Pinus silvestris*)	3	
	Common yew (*Taxus baccata*)	1	
Water repellent	Norway spruce (*Picea abies*)	1	Penetration in fibre direction
		3	Penetration perpendicular to fibre direction
	European Beech (*Fagus sylvatica*)	1	Penetration in fibre direction
		3	Penetration perpendicular to fibre direction
Wood adhesive	European Beech (*Fagus sylvatica*)	3	PUR A (low viscosity)
		3	PUR B (medium viscosity)
		3	PUR C (high viscosity)

Methods

Computed tomography is a method using information on an object obtained from different angles to produce virtual cross-sectional images of the object's inner structure.

In the present study, tomography was based on transmission images, which are shadow images of an examined object. This object attenuates the beam either by absorption or by scattering depending on its elemental composition and inner constitution. The correlation between incident/transmitted beam intensity and the material properties can be described in a first-order approach by the linear attenuation law:

$$I = I_0 \cdot e^{-\mu \cdot x}, \tag{1}$$

where I is the intensity of the transmitted beam, I_0 is the intensity of the incident beam, μ is the attenuation coefficient or macroscopic cross-section of the materials and x is the specimen thickness. The attenuation coefficient is the main value, which describes the degree to which a sample or material attenuates the incident beam. The attenuation coefficient for X-ray depends on the density as well as on the elemental composition. The interaction probability of X-ray photons with atoms of different elements is strongly correlated to the atomic number of the participating elements. For most wood species the elemental composition of wood is almost identical (C $\sim$ 50%$_{\text{weight}}$, O $\sim$ 44%$_{\text{weight}}$, H $\sim$ 6%$_{\text{weight}}$). As these are elements

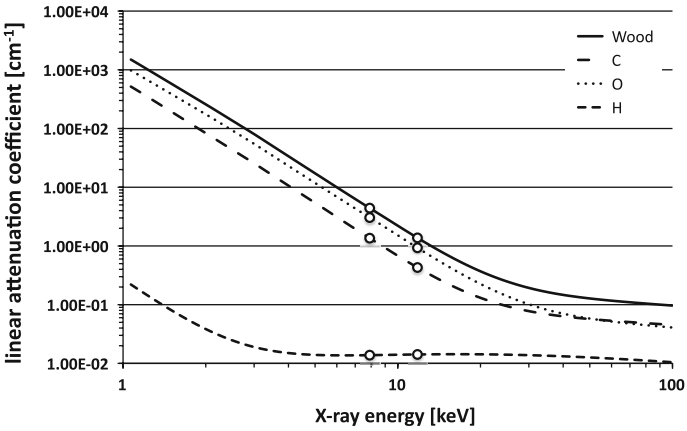

Fig. 1 The theoretical linear attenuation coefficient of wood and its three main elemental components carbon, oxygen and hydrogen (proportion taken into account) over the X-ray energy (note the double logarithmic scale) (according to Hubbell and Seltzer 2004); the emphasised points mark the two energy levels, which were used in the presented investigations

with small atomic numbers, their interaction probability is correspondingly small, which necessitates the utilisation of relatively low beam energies for investigations. An overview of the attenuation coefficients of these elements for different energy levels is given in Fig. 1 (data based on Hubbell and Seltzer 2004). The attenuation of wood in the utilised energy range mainly results from the content of O and C, while H is almost negligible.

On the basis of Eq. 1, the attenuation coefficient can be calculated from single transmission images, summarising the interaction of radiation and matter along the way of the beam through the examined object. Thus the attenuation coefficient is also found in computed tomography, which uses a multitude of transmission images to produce virtual cross-sections of an object. The resulting cross-section image can be regarded as a map of the attenuation coefficients in the respective slice yielding thus information on the material properties for every pixel in the image.

Experimental conditions

The experiments were performed at the TOMCAT beamline at the SLS (Stampanoni et al. 2007). The beamline is fed by a 2.9-T superbend with a critical energy of 11.1 keV. The energy used for the experiments can be selected with a Double Crystal Multilayer Monochromator within a range from 8 to 45 keV. The detector system consists of a scintillator-CCD-camera system. The used YAG:Ce 20 μm scintillator converts the X-ray photons into visible light projected on a 14bit-CCD-camera with 2,048 × 2,048 pixels via optical objectives.

Tomograms were acquired at 12 keV for samples with a diameter of 3 mm and at 8 keV for samples with a diameter of 1 mm. In every tomography run, 1,501 projections were collected over 180°. The distance to the detector was only few millimetres as the sample manipulator was moved to the scintillator as closely as

Table 2 Experimental conditions at TOMCAT during the experiments

Sample diameter (mm)	Beam energy (keV)	Scintillator	Field of view (mm)	Pixel size (μm)	Exposure time (ms)	Number of projections
1	8	YAG:Ce 20 μm	1.5 × 1.5	1.48 × 1.48	720	1,501
3	12		3.7 × 3.7	3.7 × 3.7	300	

possible. The field of view was adjusted to the respective sample size (3.7 × 3.7 mm^2 for the 3-mm and 1.5 × 1.5 mm^2 for the 1-mm specimens). The images were binned resulting in an effective nominal pixel size of 3.7 × 3.7 and 1.48 × 1.48 μm^2 and an exposure time of 300 and 720 ms, respectively. To correct possible inhomogeneities of the scintillator or fluctuations of the beam, every 50 projections of the sample was moved outside the field of view and two flat-field images were acquired. Table 2 gives an overview of the experimental setups.

Data reconstruction and evaluation

The tomography data were reconstructed with a software based on a Filtered-Back-Projection algorithm. The resulting data consist of stacks of cross-sectional slices stored as unsigned 16bit TIFF files.

The reconstructed images were analysed and visualised with the standard software packages *ImageJ* and *VGStudioMax*®.

Results and discussion

Anatomical features

Samples of three softwood and two hardwood species were studied with regard to the anatomical features discernible in the resulting tomography data (2D slices through the sample and a rendered visualisation of the 3D volume data set). The samples with a diameter of 3 mm and lower spatial resolution (oak and Scots pine) will be presented first, and the smaller samples with higher resolution second. For the species with two sample sizes (beech and Norway spruce) only the results of the smaller specimen and higher magnification will be presented.

Oak (Quercus sp.)

The examined 3-mm oak specimen had, as given by the detector characteristics, a nominal voxel size of 3.7 × 3.7 × 3.7 μm^3. In the cross-section, the different cell types like spring and latewood vessels are as clearly discernable as fibres and parenchyma cells (Fig. 2). The vessels are filled with tyloses (apparent thickness: 1 pixel, which corresponds to 3.7 μm, Fig. 3). While their thickness remains relatively stable, their greyscale level, which corresponds to the attenuation

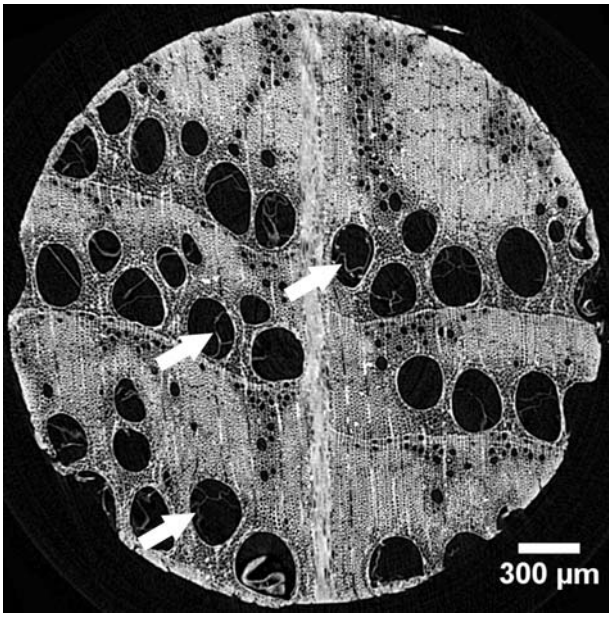

Fig. 2 Cross-section through the reconstructed tomography data of an oak specimen (*Quercus* sp.) (∅ 3 mm). The different cell types (vessels, fibres, parenchyma, etc.) are clearly discernable as well as the tyloses within the vessels (*arrows*)

coefficient of the material, differs considerably throughout the data set. According to Williams (1942), the thickness of tyloses in American oak species varies from <2 to >5µm. Some tyloses within the specimen are probably less thick than the nominal voxel size of the tomography data. The different greyscale levels suggest that it is possible to discern between thick- and thin-walled tyloses as it is unlikely that their attenuation coefficient and thus their elemental composition varies to such a degree.

The 3D disposition becomes visible after rendering the tomography data with a suitable software (Fig. 4). The polygonal shape of the tyloses can be made visible at an arbitrary position within the sample without risking possible artefacts (e.g. sectioning of microscopic samples).

The results for the oak specimen are promising especially since even structures smaller than the actual voxel size can obviously be resolved. Higher resolution could be obtained using a smaller field of view and smaller specimens, which was not attempted here. As the specimen should contain a whole annual ring, very narrow ringed oak wood was chosen. As spring vessels can be 300–400 µm in diameter, preparing a smaller specimen using a turning lathe was estimated to be impossible. An alternative preparation was described by Trtik et al. (2007), who produced prism-shaped spruce samples with a cross-sectional size of 200 µm × 200 µm and a length of several mm using a standard microtome. Another option might be local tomography, where a setup with a small field of view is used to investigate a limited section within a bigger sample (with a size larger than the actual field of view). This

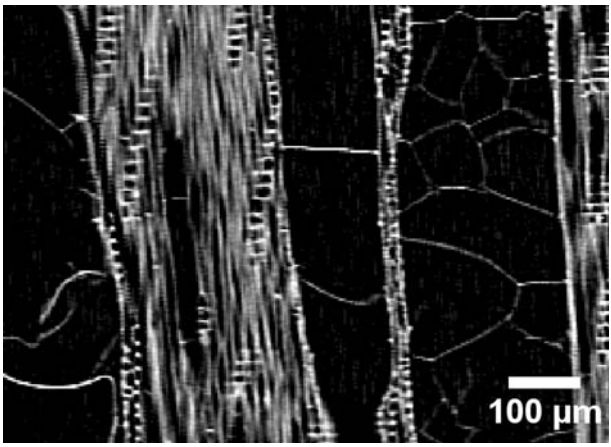

Fig. 3 Tangential slice through the reconstructed tomography data set of an oak wood sample; the tyloses show thicknesses of 3.7 µm, which represents the nominal pixel size of the experimental setup for this sample

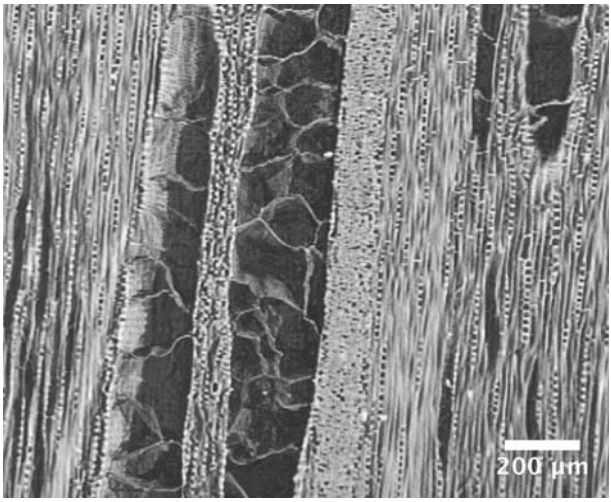

Fig. 4 Rendered 3D view of the tomography data of oak wood, showing a tangential section through the specimen; prominent are the big spring vessels filled with tyloses

method would nevertheless have disadvantages such as lower quality and artefacts in the outer region of the reconstructed data.

Scots pine (Pinus silvestris)

The cross-section of the pine sample (∅ 3 mm) shows a very narrow tree ring structure with several annual rings as well as a couple of filled and unfilled resin channels (Fig. 5). A closer look at a radial section (Fig. 6) shows the typical

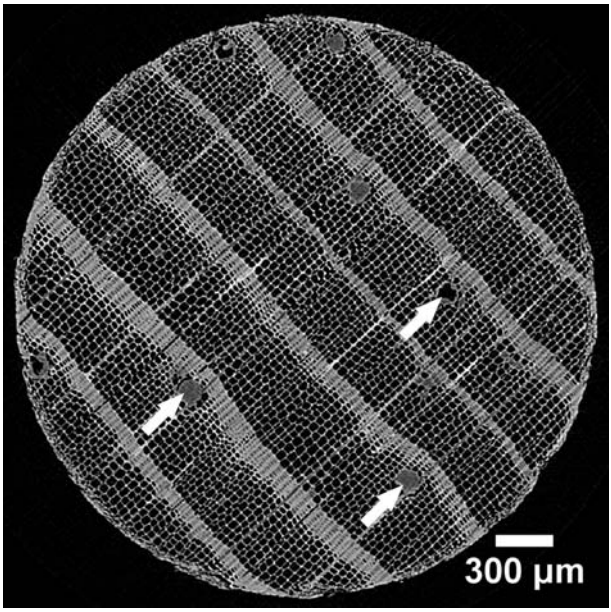

Fig. 5 Cross-section through the reconstructed tomography data set of a Scots pine specimen (*Pinus silvestris*) (∅ 3 mm) with narrow growth rings and a couple of resin channels (*arrows*)

microscopic features of Scots pine: the big window-like pits connecting ray parenchyma cells and tracheids, and ray tracheids with their dentate walls on the upper and lower boundaries of the wood ray. Although the size of these features (pits width 10–30 µm; length of dentate structures approximately 10 µm) is considerably bigger than the nominal voxel size ($3.7 \times 3.7 \times 3.7$ µm^3), they remain blurry. Smaller features could not be found due to the relatively coarse resolution. Using smaller specimens and a smaller field of view (= smaller nominal pixel size) would improve the resolution and make more details visible. The resolution is still good enough to get a good overview of the general pine wood anatomy.

European beech (Fagus sylvatica)

In the tomography data of the beech sample (∅ 1 mm), the different cell types which are typical for this species can be distinguished only to a certain degree (Fig. 7). While vessels and wood rays can be easily discerned, it is more difficult to distinguish between libriform fibres, fibre-tracheids, tracheids and axial parenchyma, which is, however, also true for standard microscopy.

The smallest detectable features are pits between vessels or fibres. In spite of their small size in the micrometre range (Jayme and Azzola 1965; Fengel 1966), they are clearly visible in the tomography slices where the nominal pixel size is only 1.48×1.48 µm^2 (Fig. 8).

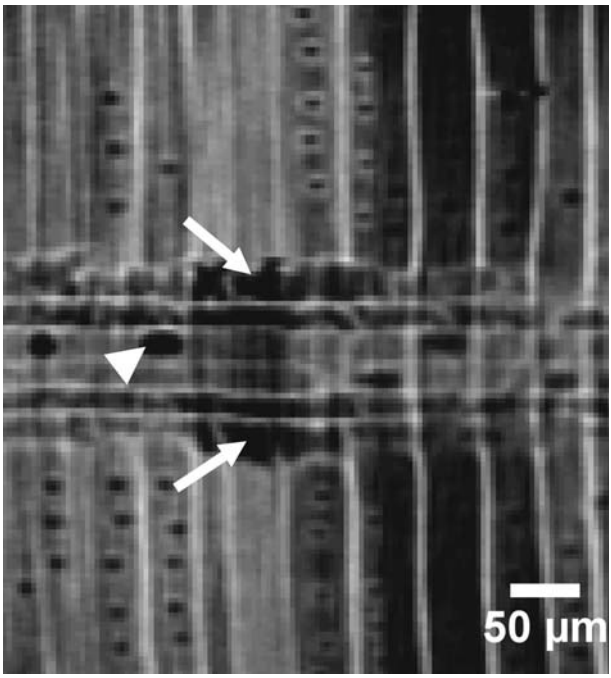

Fig. 6 Radial slice through a reconstructed tomography data set of a Scots pine specimen (*Pinus silvestris*); typical anatomical features like window pits (*arrow head*) between ray parenchyma and tracheids are visible as well as the dentate ray tracheids (*arrows*)

Common yew (Taxus baccata)

Spiral thickenings attached to the inner cell wall layer are typical microscopical features of yew tracheids. Their diameter is <1µm (Timell 1978). They were clearly visible in the reconstructed slices (Fig. 9), although their nominal pixel size is $1.48 \times 1.48\ \mu m^2$. Thus even structures with sub-voxel size can be made visible with the tomographic approach. The rendered 3D reconstruction shows the spatial disposition of the spiral thickening along the tracheids (Fig. 10).

Norway spruce (Picea abies)

The microscopical features in the reconstructed data of the Norway spruce specimen (∅ 1 mm) appear only after closer examination. Figure 11 shows a radial slice through the sample, with a partially filled resin channel on the left hand side and a wood ray in the upper part. The latter shows piceoid pits (size 2–4 µm) in the cross-fields connecting wood ray parenchyma with tracheids.

In another radial slice (Fig. 12), a torus-like structure is visible in the centre of bordered pits. Although visible in several radial sections, this structure could not be found in tangential slices. While the diameter of a torus extends to few micrometers,

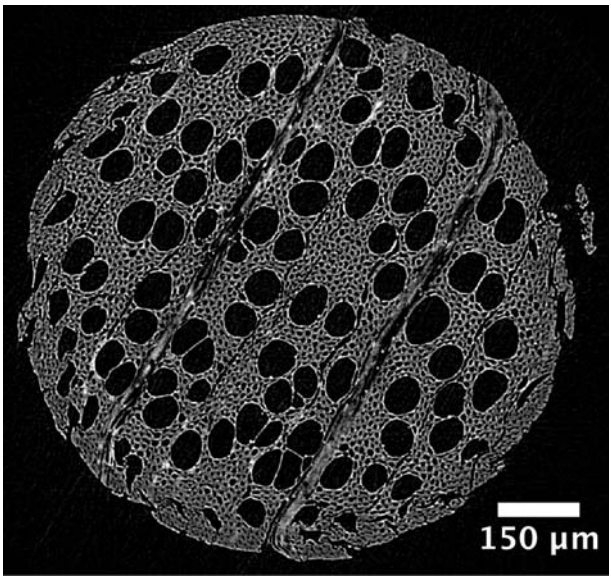

Fig. 7 Cross-section through the reconstructed tomography data of a beech specimen (*Fagus sylvatica*) (∅ 1 mm). Vessels and wood ray parenchyma are clearly discernable but it is hard to distinguish between fibres, tracheids and axial parenchyma

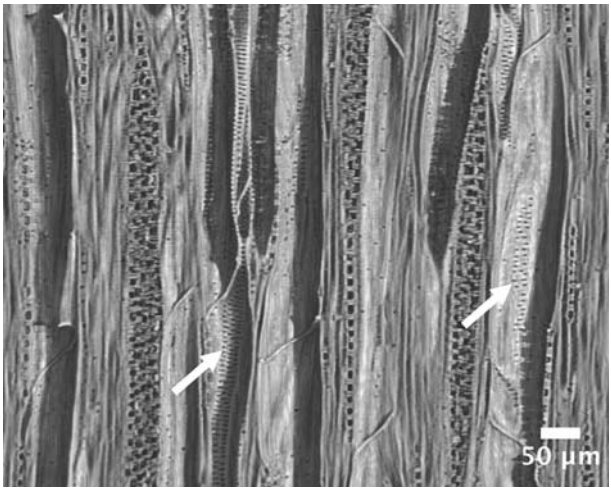

Fig. 8 Tangential cut through the 3D rendering of the tomography data set of a beech specimen (*Fagus sylvatica*); the smallest discernable anatomical features are some pits with a height of 1 pixel corresponding to a size of 1.48 µm (*arrows*)

its thickness varies between 500 nm and 1 µm (Trtik et al. 2007), which again falls below the nominal voxel size of the tomography. It is thus hard to estimate if a torus was observed or an artefact caused by the visualisation of the data.

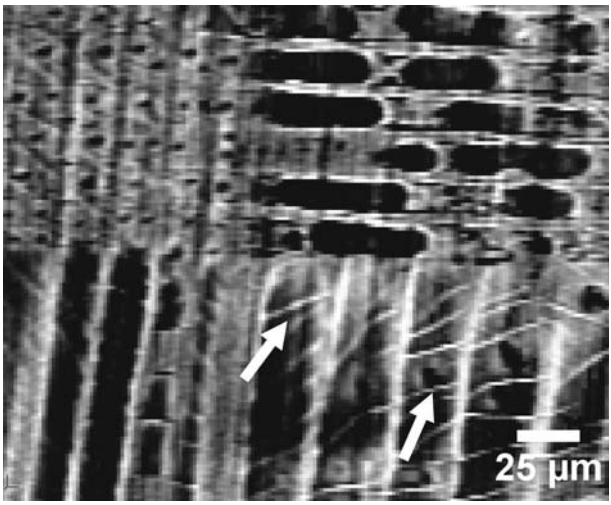

Fig. 9 Radial slice through the reconstructed tomographic data of the yew specimen (∅ 1 mm); spiral thickenings (thickness <1 µm) in the tracheids are clearly visible although the nominal pixel size is $1.48 \times 1.48\ \mu m^2$

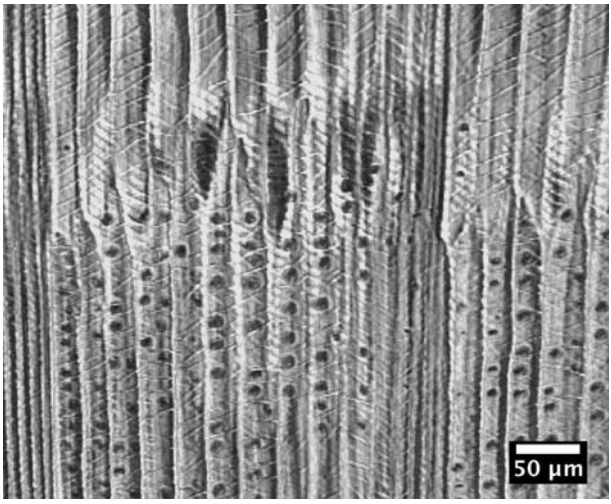

Fig. 10 Rendered 3D view of the tomography data of a yew sample (∅ 1 mm) showing tracheids with spiral thickenings, bordered pits and a year ring boundary *on the left hand side*

Penetration behaviour of a wood preservative

The samples treated with the silver-bearing water repellent showed no clear result. Due to its higher atomic number compared to the wood-composing elements, silver has a considerably higher attenuation coefficient. Thus it was expected that even small silver traces should be detectable within the tomography data.

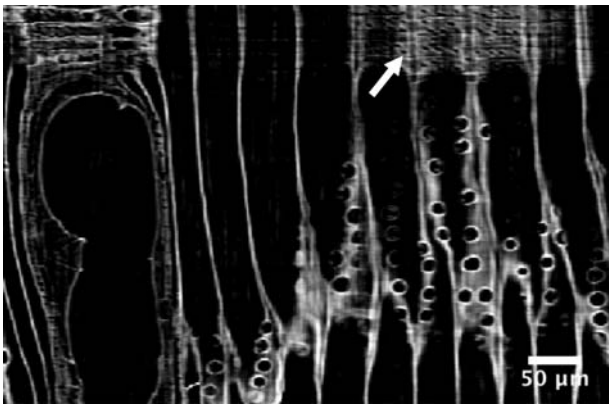

Fig. 11 Radial slice through the reconstructed tomographic data of a spruce sample (∅ 1 mm); in the upper part, piceoid pits (*arrow*) connecting a wood ray with tracheids are visible, while the *left side* of the image is occupied by a partially filled resin channel

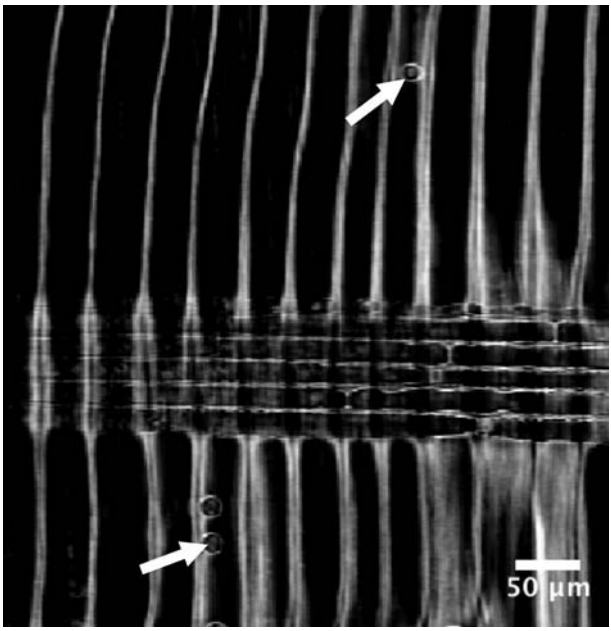

Fig. 12 Radial section through the reconstructed tomographic data of a spruce specimen (∅ 1 mm) showing ray cells and a couple of bordered pits; the bordered pits show a structure in their respective centre (*arrows*), which might be the pits torus

Both wood species (beech and spruce; cf. Table 1) as well as both fibre orientations (penetration of the water repellent in and perpendicular to the fibre orientation) showed only scarce traces of the water repellent. Only when the agent had penetrated the wood perpendicular to the fibre, the samples indicate a treatment.

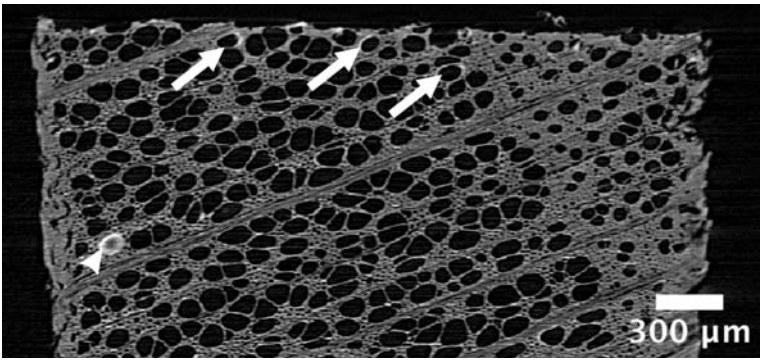

Fig. 13 Slice through the reconstructed tomography data of a beech specimen (∅ 3 mm) treated with an Ag-nano-particle-containing water repellent. Brighter areas on and near the surface (*arrows*) as well as a vessel filled (*arrow head*) with a bright substance indicate the presence of the silver-bearing preservative

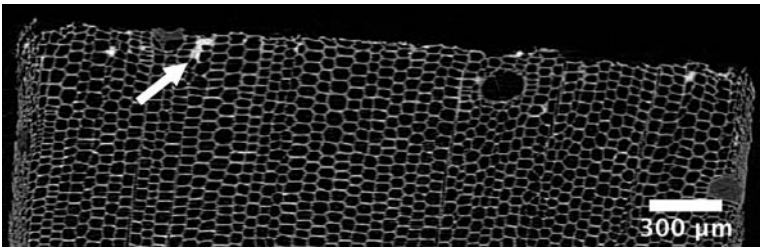

Fig. 14 Slice through the reconstructed tomography data of a spruce specimen (∅ 3 mm) treated with an Ag-nano-particle-containing water repellent. Brighter areas near the surface (*arrow*) indicate the presence of the silver-bearing preservative

The beech sample shows a single vessel (few hundred micrometres from the surface) filled with a substance with a higher attenuation coefficient than the surrounding wood. Furthermore a couple of vessels close to the surface obviously have a layer with a higher attenuation coefficient on their cell wall (Fig. 13). In the vicinity of the surface, the spruce sample shows few tracheids partially filled with a substance (Fig. 14). No convincing evidence of present water repellent was found in the remaining data. Probably the overall concentration of silver nano-particles is too low to be detected.

No qualitative or quantitative statements on the penetration behaviour of the water repellent bearing the silver nano-particles were possible. Due to the relatively low overall silver quantity, the attenuation coefficient of the water repellent is apparently similar to that of wood, which makes it difficult to detect. De Vetter et al. (2006) overcame a similar problem by doping the water repellent with a highly attenuating component. In this present study, doping with such a highly attenuating component seemed unnecessary as a similar effect was expected from the silver particles.

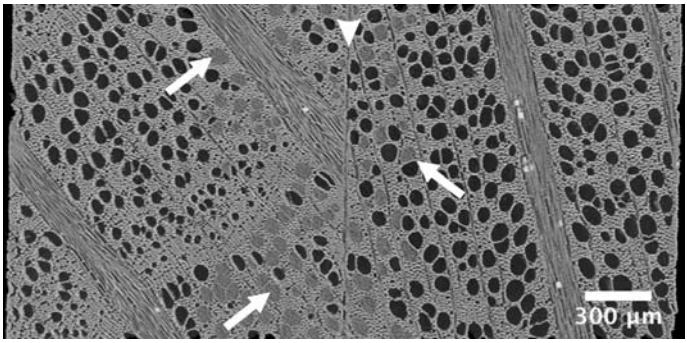

Fig. 15 Cut perpendicular to the adhesive joint (*arrow head*) through the 3D rendering of the tomographic data of a beech specimen bonded with PUR A; vessels filled with the adhesive are discernable on both sides of the joint (*arrows*)

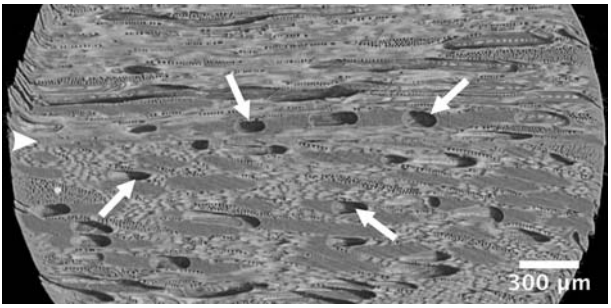

Fig. 16 Cut perpendicular to the sample axis through the 3D rendering of the tomographic data set of a beech specimen bonded with PUR A; vessels filled with the adhesive are discernable on both sides of the joint (*arrow head*); the vessels are not completely filled but show a considerable number of air bubbles (*arrows*)

Penetration behaviour of wood adhesives

The samples for examining the penetration behaviour of PUR adhesives were 3 mm in diameter. Only exemplary results for the three applied adhesives are elucidated in the following.

In the 3D reconstruction of a glued specimen, the PUR-penetrated areas are discernable both, in a view along the sample axis and perpendicular to the glue line (Fig. 15) and in a slice perpendicular to the sample axis (Fig. 16). The adhesive apparently penetrated mainly along the vessels. They are not completely filled but show many bubbles within the adhesive (probably resulting from the PUR curing).

Penetration of the adhesive into the fibre tissue could neither be proven nor be refuted. Either due to adhesive penetration or cell collapse during pressing, no fibre cell lumina were observable in the vicinity of the joint. Due to similar attenuation coefficients for the adhesive and for wood, this question cannot be answered yet. A possible way to improve the contrast might be a tomography in phase-contrast

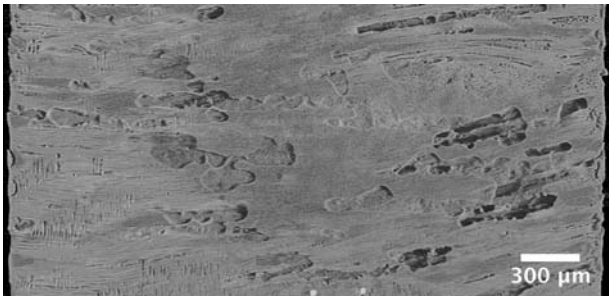

Fig. 17 Virtual cut through the adhesive joint in the 3D rendering of the tomographic data set of a beech specimen bonded with PUR A showing the distribution of the adhesive as well as flaws within the joint itself

mode, where edges are emphasised and which is particularly suitable for materials with low attenuation coefficients. Alternatively, neutron tomography might yield a better contrast than X-ray since neutrons are more sensitive for hydrogen. However, the spatial resolution (few tens of micrometres) is here still too low to attend the cellular wood level, so neutron tomography could only yield an impression of the mean adhesive distribution near the joint.

Tomography enables to arbitrarily lay virtual sections through the sample. Figure 17 shows a viewing plane lying parallel within the adhesive joint. It is thus possible to examine the distribution of the adhesive within the intact joint, to estimate the area which is actually covered by the adhesive, and to identify flaws in the adhesive bondline.

Sample preparation

Preparing samples with a turning lathe was a fast and trouble-free procedure. Except for ring-porous species with wide vessels, diameters down to 1 mm are feasible. For smaller samples, alternative preparation methods (Trtik et al. 2007) seem more appropriate.

The preparation barely seemed to affect the samples. Only close to the outer brim, the cylindrical samples show plastic deformation caused by machining.

Thus the chosen method allows producing plenty of high-quality samples in reasonable time.

Conclusion

Synchrotron radiation micro computer tomography is a suitable method for non-destructive evaluation of wood on the microscopic level. Both anatomical and technical wood issues can be examined, although the method appears more appropriate for some questions (penetration of adhesive) than for others (water repellent).

Synchrotron radiation micro computer tomography is applicable as alternative to light or scanning electron microscopy. Although the nominal pixel size reached in this presented study (1.48 μm) is still below that of the abovementioned standard methods, it seems possible to increase resolution. This could be achieved by using either a smaller field of view or by simply acquiring the transmission data without binning while using the same field of view (nominal pixel size 0.74 μm). Yet, the method has a couple of advantages over standard microscopy. It is possible to choose the point of view within the 3D data set arbitrarily; the risk of preparation artefacts is low and the preparation less complex and less time consuming than it is for microscopy.

Acknowledgments The authors express their thanks to Mr G. Mikuljan for his help in the sample preparation and Dr D. Keunecke, Mr P. Hass and Ms Y. Herbers for their assistance during the measurements.

References

Bucur V (2003a) Techniques for high resolution imaging of wood structure: a review. Meas Sci Technol 14:R91–R98

Bucur V (2003b) Non-destructive characterisation and imaging of wood. Springer, Berlin

De Vetter L, Cnudde V, Masschaele B, Jacobs PJS, Van Acker J (2006) Detection and distribution analysis of organosilicon compounds in wood by means of Sem-Edx and Micro-Ct. Mater Charact 56:39–48

Dodd JD (1948) On the shapes of cells in the cambial zone of *Pinus silvestris* L. Am J Bot 35:666–682

Donaldson LA, Lausberg MJF (1998) Comparison of conventional transmitted light and confocal microscopy for measuring wood cell dimensions by image analysis. IAWA J 19(3):321–336

Fengel D (1966) Electron microscopic contributions to the fine structure of beechwood (*Fagus sylvatica* L.)—part III: the fine structure of the pits in beechwood. Holz Roh Werkst 24(6):245–253

Groso A, Abela R, Stampanoni M (2006) Implementation of a fast method for high resolution phase contrast tomography. Opt Express 14(18):8103–8110

Hubbell JH, Seltzer SM (2004) Tables of X-ray mass attenuation coefficients and mass energy-absorption coefficients, version 1.4. National Institute of Standards and Technology, Gaithersburg. Available online at: http://physics.nist.gov/xaamdi. Cited 15 July 2008

Jayme G, Azzola FK (1965) Texture and topochemistry of beechwood pits and pitmembranes (*Fagus sylvatica* L.). Holz Roh Werkst 23:41–49

Kitin P, Sano Y, Funada R (2003) Three-dimensional imaging and analysis of differentiating secondary xylem by confocal microscopy. IAWA J 24(3):211–222

Kitin P, Fujii T, Abe H, Funada R (2004) Anatomy of the vessel network within and between tree rings of *Fraxinus lanuginosa* (Oleaceae). Am J Bot 91(6):779–788

Knebel W, Schnepf E (1991) Confocal laser scanning microscopy of fluorescently stained wood cells: a new method for three-dimensional imaging of xylem elements. Trees 5:1–4

Macedo A, Vaz CMP, Pereira JCD, Naime JM, Cruvinel PE, Crestana S (2002) Wood density determination by X- and gamma-ray tomography. Holzforschung 56(5):535–540

Mannes D, Lehmann E, Niemz P (2007) Tomographic investigations of wood from macroscopic to microscopic scale. In: Proceedings of the 15th symposium on non-destructive wood testing. Natural Resources Research Institute, University of Minnesota, Duluth and USDA Forest Products Laboratory

Niemz P, Mannes D, Haase S, Lehmann E, Vontobel P (2004) Untersuchungen zur Verteilung des Klebstoffes im Bereich der Leimfuge mittels Neutronenradiographie und Mikroskopie. Holz Roh Werkst 62:424–432

Stampanoni M, Groso A, Isenegger A, Mikuljan G, Chen Q, Meister D, Lange M, Betemps R, Henein S, Abela R (2007) TOMCAT: a beamline for tomographic microscopy and coherent radiology experiments. Synchrotron Radiat Instrum 879(Pts 1–2):848–851

Steppe K, Cnudde V, Girard C, Lemeur R, Cnudde JP, Jacobs P (2004) Use of X-ray computed microtomography for non-invasive determination of wood anatomical characteristics. J Struct Biol 148:11–21

Timell TE (1978) Helical thickenings and helical cavities in normal and compression woods of *Taxus baccata*. Wood Sci Technol 12(1):1–15

Trtik P, Dual J, Keunecke D, Mannes D, Niemz P, Stähli P, Kaestner A, Groso A, Stampanoni M (2007) 3D imaging of microstructure of spruce wood. J Struct Biol 159:46–55

Van den Bulcke J, Masschaele B, Dierick M, Van Acker J, Stevens M, Hoorebeke Van (2008) Three-dimensional imaging and analysis of infested coated wood with X-ray submicron CT. Int Biodeterior Biodegradation 61:278–286

Williams S (1942) Secondary vascular tissues of the oaks indigenous to the United States—II. Types of tyloses and their distribution in Erythrobalanus and Leucobalanus. Bull Torrey Bot Club 69(1):1–10